

12-1-2020

Vibration Overtone Hyperpolarizability Measured for H₂ Using Electric Field Induced Second Harmonic Generation

Rachel Ellis

Follow this and additional works at: <https://digitalscholarship.unlv.edu/thesesdissertations>



Part of the [Optics Commons](#)

Repository Citation

Ellis, Rachel, "Vibration Overtone Hyperpolarizability Measured for H₂ Using Electric Field Induced Second Harmonic Generation" (2020). *UNLV Theses, Dissertations, Professional Papers, and Capstones*. 4050. <https://digitalscholarship.unlv.edu/thesesdissertations/4050>

This Thesis is protected by copyright and/or related rights. It has been brought to you by Digital Scholarship@UNLV with permission from the rights-holder(s). You are free to use this Thesis in any way that is permitted by the copyright and related rights legislation that applies to your use. For other uses you need to obtain permission from the rights-holder(s) directly, unless additional rights are indicated by a Creative Commons license in the record and/or on the work itself.

This Thesis has been accepted for inclusion in UNLV Theses, Dissertations, Professional Papers, and Capstones by an authorized administrator of Digital Scholarship@UNLV. For more information, please contact digitalscholarship@unlv.edu.

VIBRATION OVERTONE HYPERPOLARIZABILITY MEASURED FOR H₂
USING ELECTRIC FIELD INDUCED SECOND HARMONIC GENERATION

By

Rachel M. Ellis

Bachelor of Science – Physics
University of Nevada, Las Vegas
2017

A thesis submitted in partial fulfillment
of the requirements for the

Master of Science – Physics

Department of Physics and Astronomy
College of Sciences
The Graduate College

University of Nevada, Las Vegas
December 2020

Copyright

Copyright [2021] by [Rachel Ellis]

All Rights Reserved



Thesis Approval

The Graduate College
The University of Nevada, Las Vegas

November 13, 2020

This thesis prepared by

Rachel M. Ellis

entitled

Vibration Overtone Hyperpolarizability Measured for H₂ Using Electric Field Induced
Second Harmonic Generation

is approved in partial fulfillment of the requirements for the degree of

Master of Science - Physics
Department of Physics and Astronomy

David Shelton, Ph.D.
Examination Committee Chair

Kathryn Hausbeck Korgan, Ph.D.
Graduate College Dean

Victor Kwong, Ph.D.
Examination Committee Member

Bernard Zygelman, Ph.D.
Examination Committee Member

Clemens Heske, Ph.D.
Graduate College Faculty Representative

Abstract

The vibrational contribution to the second hyperpolarizability (γ) of gas phase H_2 was measured using electric field induced second harmonic generation. Measurements were made for the pure vibrational 3-0 Q(J) overtone transitions ($v=0,J \rightarrow v'=3,J$ for $J = 0,1,2,3$). Measured intensities were found to be 4-14% larger than *ab initio* calculations. The first chapter of this thesis provides an introduction to nonlinear optics, second harmonic generation, and the tensor nature of hyperpolarizabilities. The second chapter provides theoretical expressions for γ and relevant static and Raman polarizabilities. The third chapter covers the experimental design and electric field induced second harmonic generation. The final two chapters discuss the results and analysis of the experiment and possible future impact.

Acknowledgements

I would like to acknowledge Dr. David Shelton who spent countless hours explaining and teaching the content necessary for this thesis project to get off the ground. I would also like to acknowledge my committee members Dr. Bernard Zygelman, Dr. Victor Kwong, and Dr. Clemens Heske who have all helped me progress as a researcher and have been nothing but kind. Further, I would like to thank Dr. Jeff Wragg for being kind enough to go out on a limb and look over my manuscript, despite being states away. I owe the largest of thanks to the support of my family and to Sterling Hall, all of who have listened to me talk about lasers for the last 3 years.

Contents

Abstract	iii
Acknowledgements	iv
Contents	vi
List of Tables	vii
List of Figures	viii
1 Introduction	1
1.1 A Very Brief History of Nonlinear Optics	1
1.2 Molecular Polarizability and Polarization	2
1.3 The Second Hyperpolarizability, Gamma	5
1.4 Definitions and Units	6
2 Theory	9
2.1 Perturbation Theory and the Sum-Over-States Description	9
2.2 Approximation, Q-Branch, S-branch, O-branch Vibrational Hyperpolarizability	14
2.3 Microscopic Approximation, γ_{res}	16
2.4 Static and Dynamic Polarizabilities	17
3 Experimental Design	19
3.1 Design and Set Up	19
3.2 Signal Collection: Photon Counting Statistics	22
3.3 Measurement Process: Singlets, Triplets, and Power	23
3.4 Coherent Background	24
3.5 Electric Field Induced Second Harmonic Generation, Phase-match Peak . . .	24
3.6 Resonant Fit Function	27

4	Analysis and Results	30
4.1	Collisional Broadening	30
4.2	Effective Polarizability and Non-Resonance Response	30
4.3	Comparing Relative Strength of Resonance	34
4.4	Data Analysis: Effective Polarizability	34
4.5	Data Analysis: Non-resonant Contributions	35
5	Conclusion	37
	Bibliography	42
	Curriculum Vitae	43

List of Tables

Table 1	Polarization Units	6
Table 2	Common nonlinear optical processes and accompanying papers	7
Table 3	Experimental results of the fit function Equation 44	29
Table 4	Pressure shift and broadening coefficients measured for H ₂ vibration transitions.	31
Table 5	Parameters for Equation 50	33
Table 6	Comparison for experimental and calculated resonance at T=295 K	34

List of Figures

Figure 1	Molecular frame of reference	8
Figure 2	Transition diagram	14
Figure 3	Laser cavity diagram	20
Figure 4	Schematic diagram of experimental set up	21
Figure 5	ESHG signal vs frequency measured for the H ₂ 3-0 Q(1) transition . .	26
Figure 6	Resonance spectra for Q (0), Q (1), Q _⊥ (1), Q (2),Q (3)	28
Figure 7	Pressure shift and broadening coefficients	32

1 Introduction

This thesis presents the results of an investigation into the second hyperpolarizability (γ) of H_2 gas using electric field induced second harmonic generation (ESHG). In order to appreciate the findings, an introduction to nonlinear optics (NLO) is required. This introduction chapter will cover a very brief history of NLO, molecular polarization and polarizability, a simple description of the second hyperpolarizability, and finally will provide a guide to tensors, abbreviations, and units used to explain such phenomena along with their typical sizes.

Beyond this introductory chapter there are four additional chapters. These four additional chapters are: first, the theoretical foundation for γ mediating second harmonic generation along with static and dynamic polarizabilities; next, a description of the experimental set-up including spectral resolution, noise reduction techniques, and a description of the technique of electric field induced second harmonic generation; then, the results and analysis of the experiment including pressure shifts and *ab initio* comparisons of Raman polarizabilities; finally, closing remarks and possible applications of the experimental method used are provided.

1.1 A Very Brief History of Nonlinear Optics

Optical tools and theory have existed in various cultures throughout time, from Mesopotamia ($\sim 4,000$ BCE), as evidenced by the archaeological discoveries of polished rock-crystal lenses [1], to Epicurus of Samos (340-270 BCE) in ancient Greece, who wrote about relations between light and color [2]. In the West, theoretical and experimental investigations of optics expanded during the European Enlightenment period (~ 1685 -1815) with the theories of Newton, Kepler, and Euler [3]. Nonlinear electromagnetic phenomena have been investigated since the discovery of iron's nonlinear response to an external magnetic field in the 19th century [4] and was furthered by the formalization of quantum mechanics in the 20th century, which led to the development of (nonlinear) quantum optics. For a more in-depth

investigation of the history of optics see Olivier Darrigol's *A History of Optics, From Greek Antiquity to the Nineteenth Century* [5].

The study of quantum optics was advanced with the invention of the laser in 1960 by Theodore Maiman [6], which allowed for the creation of a high powered (intense) coherent light source necessary for NLO investigations. The NLO phenomenon of interest to this thesis, second harmonic generation, was theoretically predicted in 1931 by Maria Göppert-Mayer [7], and was first experimentally observed in 1961 by Franken et al [8]. Sum frequency generation (SFG), which is the broader category that second harmonic generation (SHG) belongs to, is primarily of interest for frequency conversion (for which crystals and condensed phase materials are preferred for applications), while other applications in biological research [9] (SHG microscopy, THG microscopy), quantum information [10] (parametric amplification in fibers), and device production [11] (lasers, optical devices such as phase conjugate mirrors) also contribute to the widespread interest in sum frequency generation. While early research focused on nonlinear effects in crystals lacking centro-symmetry, such research was stymied by absorption effects and high intensity surface damages, reducing the number of usable materials for various applications [12]. The shift in NLO research from crystals to gas and vapors has allowed for a wider range of investigation for light and molecules.

1.2 Molecular Polarizability and Polarization

Molecular optics studies the way in which the electromagnetic field of light manipulates charge within materials. There are two major considerations when discussing molecular optics, the way to think about the electromagnetic field (classical, quantum) and the strength of the electromagnetic field.

Consider the applied electromagnetic field in terms of a photon with momentum $p = E/c$ interacting with a single molecule: the photon's momentum will transiently be transferred to the molecule but will not excite the molecule and so there will be almost no energy transfer between the photon and molecule (Rayleigh scattering). At the instant of momentum transfer

the photon is considered to be absorbed and the molecule is in a virtual state – that is the molecule is in a superposition of stationary states. The virtual state does not last forever and as a result of this decay, a scattered photon with the same energy as the incident photon’s energy is produced when the molecule transitions from the virtual state to its initial state. Momentum transfer between a photon and a molecule is not restricted to one photon at a time and a stronger electric field will increase the probability of multi-photon interactions with a single molecule. Multi-photon interactions give rise to frequency mixing such as SHG where two photons of equal frequency are absorbed and from this, a photon with twice the frequency is generated.

Considering the applied electromagnetic field in terms of a plane wave, the coupling between the field and the molecule can be approximated as a classical dipole interaction with the field inducing a time-dependent polarization of the molecule. Such interactions can be expressed mathematically by a Taylor series approximation of the electric dipole moment $\bar{\mu}$ which is induced by an applied electric field E_j

$$\mu_i = \mu_i^{(0)} + \alpha_{ij}E_j + \frac{1}{2!}\beta_{ijk}E_jE_k + \frac{1}{3!}\gamma_{ijkl}E_jE_kE_l + \dots, \quad (1)$$

where μ_i is the Cartesian component i of the total induced dipole moment, $\mu_i^{(0)}$ is the permanent (unperturbed) dipole moment of the molecule, α_{ij} is the linear polarizability tensor, β_{ijk} is the first hyperpolarizability tensor, γ_{ijkl} is the second hyperpolarizability tensor, and so on. E_j are components of the applied electric field. The nonlinear polarizability tensors ($\beta_{ijk}, \gamma_{ijkl}$) allow for a more accurate description of the total induced dipole moment when larger electric fields are applied to the molecule.

Physically, Equation 1 can be visualized as light traveling through a medium, where the light’s electromagnetic field interacts with the medium’s charges. Equation 1 breaks down for applied electric fields stronger than the atom’s Coulomb field, which for H_2 , is $\sim 1.6 \times 10^{11}$ V/m. The applied electric field used for this thesis was $\sim 19.5 \times 10^5$ V/m.

The induced dipole expressed by Equation 1 depends on local fields experienced by the molecule. For the present experiment, local fields and the applied electric field are of the same order [13]. This can be seen by considering the Lorentz local field factors necessary for relating the microscopic effects to macroscopic effects. That is, the third-order susceptibility, $\chi^{(3)}$, is related to the second hyperpolarizability, γ , by

$$\chi^{(3)} = \frac{1}{4} \left(\frac{n_0^2 + 2}{3} \right) \left(\frac{n_\omega^2 + 2}{3} \right)^2 \left(\frac{n_{2\omega}^2 + 2}{3} \right) \gamma \rho, \quad (2)$$

where n_ω and $n_{2\omega}$ are the refractive indices related to the incident and second harmonic frequencies, n_0 is the zero frequency refractive index, ρ is the number density of the gas molecules and the factor $\frac{1}{4}$ is associated with second harmonic generation. The Lorentz local field factors for dilute non-polar gas are $\mathbb{L}(\omega) = \frac{n_\omega^2 + 2}{3}$, $\mathbb{L}(2\omega) = \frac{n_{2\omega}^2 + 2}{3}$ and for the static field, $\mathbb{L}(0) = \frac{n_0^2 + 2}{3}$. The Lorentz local field factors for H_2 are $\frac{n^2 + 2}{3} \approx 1$ since $n - 1 = \frac{\rho\alpha}{3\epsilon_0} \ll 1$, for α in SI units of Table 1, these field factors are accurate due to the molecular density ρ being small enough. Physically the microscopic polarizability is a molecule-level characteristic and is a measure of charge displacement per molecule while the bulk polarization can be regarded as a density of dipoles.

The macroscopic polarization using macroscopic fields is

$$P_I = \epsilon_0 [\chi_{IJ}^{(1)} E_J + \chi_{IJK}^{(2)} E_J E_K + \chi_{IJKL}^{(3)} E_J E_K E_L + \dots], \quad (3)$$

where P_I is the macroscopic (bulk) polarization in the lab frame coordinate direction I , ϵ_0 is the permittivity of free space, $\chi_{IJ}^{(1)}$ is the first order dielectric susceptibility tensor, $\chi_{IJK}^{(2)}$ is the second order and so on, with E_J being the macroscopic electric field [14]. The susceptibilities are measures of how responsive the material is to an applied electric field.

1.3 The Second Hyperpolarizability: γ

For a centrosymmetric molecule such as H_2 , which has no permanent dipole moment ($\mu_i^{(0)}$) and no first order hyperpolarizability (β), the nonlinear response can be described by the second hyperpolarizability tensor (γ). The second hyperpolarizability $\gamma_{ijkl}(-\omega_\sigma; \omega_1, \omega_2, \omega_3)$ is a function of the incident electric field frequencies ($\omega_1, \omega_2, \omega_3$) and the polarizations (i, j, k, l) and is generated by the induced electronic, vibrational, and rotational motion of the molecule. While molecules of non-centrosymmetric and poly-atomic nature are beyond the scope of this thesis, an in-depth discussion on their treatment can be found in Shelton and Rice’s “Measurements and Calculations of the Hyperpolarizabilities of Atoms and Small Molecules in the Gas Phase” [15].

Continuing the discussion for centrosymmetric molecules like H_2 , an invocation of the Born-Oppenheimer approximation entails that its hyperpolarizability can be examined in two distinct ways, electronically and vibrationally [16]. This distinction draws from the very different time scale for response of the nucleus and electrons meaning: 1) the electronic hyperpolarizability is a measure to quantify the effect the applied electric fields have on the motion of electrons while neglecting nuclear motion and 2) the vibrational hyperpolarizability quantifies the effects from geometric changes of the nuclear frame that the electrons adiabatically follow.

The electronic contribution to the hyperpolarizability of a molecule has been studied extensively and can generally be described by a single dispersion formula, regardless of NLO process, at frequencies well below the first electronic resonance. For the case where the optical and static electric fields are polarized in parallel to one another, the second hyperpolarizability electronic frequency dispersion formula is determined to be [15]

$$\gamma_{\parallel}^e(-\nu_\sigma; \nu_1, \nu_2, \nu_3) = \gamma_{\parallel}^e(0; 0, 0, 0) \times (1 + A\nu_L^2 + B\nu_L^4 + C\nu_L^6 + \dots), \quad (4)$$

where $\nu_\sigma = \sum_i \nu_i$ and $\nu_L^2 = \nu_\sigma^2 + \nu_1^2 + \nu_2^2 + \nu_3^2$. For this experiment, electric field induced second

harmonic generation, $\nu_1 = \nu_2$, and $\nu_3 = 0$, and $\nu_L^2 = 6\nu^2$. The component $\gamma_{\parallel}^e(0; 0, 0, 0)$ is the parallel component of the electronic hyperpolarizability for the static limit. The coefficients A, B, and C have been derived and defined by Shelton and Rice [15].

This universality is not seen for the vibrational contribution. The reason for this is that the frequency dependence for γ^v is often more complex with resonant frequencies overlapping oscillating frequencies.

1.4 Definitions and Units

To avoid any confusion between the cited literature and this work there will be a brief explanation of abbreviations, definitions, and units. Table 1 outlines each polarizability up to the third order and their subsequent units. In this text, the values for γ and α are reported in atomic units unless stated otherwise. In most cited literature, SI units were invoked and conversion may be necessary for comparison.

Table 1: Polarization Units

Polarizability	Tensor Rank	Linearity	atomic units	SI units	electrostatic units
first order, α	2	linear	$1 e^2 a_0^2 E_h^{-1}$	$1.648\ 778 \times 10^{-41} \text{C}^2 \text{m}^2 \text{J}^{-1}$	$1.481\ 7 \times 10^{-25} \text{cm}^3$
second order, β	3	nonlinear	$1 e^3 a_0^3 E_h^{-2}$	$3.206\ 361 \times 10^{-53} \text{C}^3 \text{m}^3 \text{J}^{-2}$	$8.639\ 2 \times 10^{-33} \text{cm}^4 \text{statvolt}^{-1}$
third order, γ	4	nonlinear	$1 e^4 a_0^4 E_h^{-3}$	$6.235\ 377 \times 10^{-65} \text{C}^4 \text{m}^4 \text{J}^{-3}$	$5.036 \times 10^{-40} \text{cm}^5 \text{statvolt}^{-2}$

It is important to note that the polarizability tensors and the susceptibility tensors in Equation 1 and Equation 3 are frequency dependent. For example, the second order hyperpolarizability γ_{ijkl} should be read as $\gamma_{ijkl}(-\omega_\sigma; \omega_1, \omega_2, \omega_3)$ which is the fourth rank tensor describing the optical process where an induced polarization of frequency ω_σ is produced as a result of the action of the three electric field photons of frequencies $\omega_1, \omega_2, \omega_3$ incident on

the molecule.

Two things must be mentioned for frequency: 1) following traditional notation, the leading frequency (the induced polarization frequency) is denoted by a negative value and is the sum of the frequencies of the fields associated with the polarizability coefficients (α, β, γ) and 2) different NLO processes are recognized by different field frequency compositions. For the process used in this experiment, ESHG, the frequencies are,

$$\omega_1 = \omega_2; \omega_3 = 0 \longrightarrow -\omega_\sigma = -2\omega \quad (5)$$

Table 2 shows different NLO processes listed by type, identifying frequencies, and papers for specific nonlinear events have been listed for those that are curious (though this extends beyond what is needed for understanding this thesis).

Table 2: Common nonlinear optical processes and accompanying papers

NLO Process	ω_σ	ω_1	ω_2	ω_3	Early Experiments
second harmonic generation	-2ω	ω	ω	N/A	“Generation of Optical Harmonics” [8]
electric field induced second harmonic generation	-2ω	ω	ω	0	“dc-Induced Optical Second-Harmonic Generation in the Inert Gases” [17]
third harmonic generation	-3ω	ω	ω	ω	“Optical Third Harmonic Generation in Gases by a Focused Laser Beam” [18]
optical Kerr effect	$-\omega$	ω	ω	$-\omega$	“Optical Kerr effect in liquids” [19]

To distinguish frames of reference different subscript notations are used. Up to this point, for molecule frames of reference, the microscopic polarizability tensor component has been

specified by subscripts i, j, k, l which define, along the frame of reference, the molecular axis along which polarization occurs and the directions of the pertinent applied fields [20]. For the laboratory frame of reference, the polarizability tensor component has been specified by the capitalized subscripts I, J, K, L . The molecular frame of reference is set such that the z-axis is parallel to the molecular bond (see Figure 1) while the lab frame of reference involves averaging over all possible orientations.

In the following chapters, to comply with accepted notation the tensor subscripts will be $\alpha, \beta, \gamma, \delta$ in place of i, j, k, l for molecule frame of reference. To distinguish lab frames of reference A, B, Γ, Δ for I, J, K, L is used in this thesis.

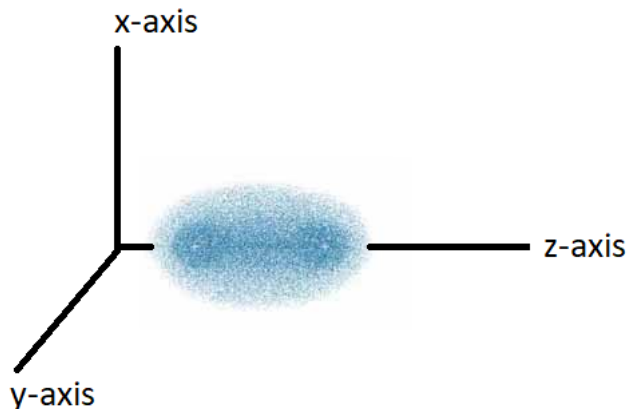


Figure 1: Molecular frame of reference, for $\gamma_{\alpha,\beta,\gamma,\delta} = \gamma_{xxxx} = \gamma_{yyyy} \neq \gamma_{zzzz}$

2 Theory

The purpose of this chapter is to expand upon the theory of hyperpolarizability introduced in the previous chapter. This chapter will cover the following topics: perturbation theory applied to the total dipole moment (Section 2.1), the Q-branch, S-branch, and O-branch approximations derived from the total second-hyperpolarizability (Section 2.2), the vibrational resonance approximation derived from the total second-hyperpolarizability (Section 2.3), and finally, static and dynamic linear polarizabilities (Section 2.4).

2.1 Perturbation Theory and the Sum-Over-States Description

The aim of this section is to develop and present an expression for the second hyperpolarizability γ using perturbation theory. Since deriving the second hyperpolarizability would take up too much time and has been derived elsewhere [21][22], the linear polarizability will be derived under a similar process as an example to establish the sum over states description.

The time-dependent Schrödinger equation (TDSE) for a time-dependent state vector $|\Psi\rangle$ is

$$\frac{\partial}{\partial t} |\Psi\rangle = (i\hbar)^{-1} \hat{H}(t) |\Psi\rangle, \quad (6)$$

where the time-dependent Hamiltonian $\hat{H} = \hat{H}^{(0)} + \lambda\hat{V}(t)$ is a summation of the unperturbed Hamiltonian $\hat{H}^{(0)}$ and the time-dependent perturbation $\lambda\hat{V}(t)$. The adjustable parameter, λ , varies from 0 to 1 with $\lambda = 0$ being an unperturbed system and $\lambda = 1$ a fully perturbed system. Using perturbation theory the wavefunction solution to the TDSE is expressed in the form of a power series expansion in λ expressed as

$$|\Psi\rangle = |\Psi^{(0)}\rangle + \lambda|\Psi^{(1)}\rangle + \lambda^2|\Psi^{(2)}\rangle + \dots + \lambda^N|\Psi^{(N)}\rangle. \quad (7)$$

Substituting Equation 7 into Equation 6 and collecting terms of like degree in λ leads to

the equations

$$i\hbar \frac{\partial}{\partial t} |\Psi^{(0)}\rangle = \hat{H}^{(0)} |\Psi^{(0)}\rangle \quad (8)$$

and

$$i\hbar \frac{\partial}{\partial t} |\Psi^{(N)}\rangle = \hat{H}^{(0)} |\Psi^{(N)}\rangle + \hat{V} |\Psi^{(N-1)}\rangle, \quad (9)$$

where $N = 1, 2, 3, \dots$ Equation 8 is the Schrödinger equation for a molecule with no externally applied field and Equation 9 is a recursion relation for the N -th order correction to the wavefunction in terms of the $(N-1)$ -th order correction, for a molecule interacting with an applied field. The solution to Equation 8 with the system assumed to be in the ground state $|g\rangle$ is

$$|\Psi^{(0)}\rangle = \exp(-i\omega_g t) |g\rangle. \quad (10)$$

For Equation 9, $|\Psi^{(N)}\rangle$ is solved by making use of the fact that the energy eigenfunctions for $\hat{H}^{(0)}$ constitutes a complete set of basis functions, and so

$$|\Psi^{(N)}\rangle = \sum_l a_l^{(N)}(t) \exp(-i\omega_l t) |l\rangle. \quad (11)$$

Substituting Equation 11 into Equation 9 where $a_l^{(N)}$ are to be determined gives

$$i\hbar \sum_l \dot{a}_l^{(N)}(t) \exp(-i\omega_l t) |l\rangle = \sum_l a_l^{(N-1)}(t) \exp(-i\omega_l t) \hat{V} |l\rangle. \quad (12)$$

The above expression can be simplified by multiplying the entire expression by $\langle m|$ and integrating over all-space, with $\langle m|l\rangle = \delta_{ml}$ leading to

$$\dot{a}_m^{(N)}(t) = (i\hbar)^{-1} \sum_l a_l^{(N-1)}(t) V_{ml}(t) \exp(i\omega_{ml} t) \quad (13)$$

or

$$a_m^{(N)}(t) = (i\hbar)^{-1} \sum_l \int_{-\infty}^t dt' a_l^{(N-1)}(t') V_{ml}(t') \exp(i\omega_{ml}t'), \quad (14)$$

where the transition frequency is denoted by $\omega_{ml} = \omega_m - \omega_l$ and the matrix element of the interaction Hamiltonian is $V_{ml} = \langle m | \hat{V} | l \rangle$.

The zeroth order probability amplitude corresponding to the system being in the ground state is $a_l^{(0)} = \delta_{lg}$. For finding higher order probability amplitudes the optical field and interaction Hamiltonian must be defined. The time varying optical field introduced to the system is defined as

$$\bar{E}(t) = \sum_p \mathbf{E}_0(\omega_p) \exp(-i\omega_p t), \quad (15)$$

the interaction Hamiltonian defined as $\hat{V} = -\hat{\mu} \cdot \bar{E}(t)$ is then,

$$V_{ml}(t) = - \sum_p \mu_{ml} \cdot \mathbf{E}_0(\omega_p) \exp(-i\omega_p t). \quad (16)$$

Plugging these definitions into Equation 14 the first-order amplitude leads to

$$a_m^{(1)}(t) = \hbar^{-1} \sum_p \frac{\mu_{mg} \cdot \mathbf{E}_0(\omega_p)}{\omega_{mg} - \omega_p} \exp(i(\omega_{mg} - \omega_p)t). \quad (17)$$

Additionally, the expectation value of the electric dipole moment per molecule (linear in the applied electric field) can be written as

$$\langle \mu^{(1)} \rangle = \langle \Psi^{(0)} | \mu | \Psi^{(1)} \rangle + \langle \Psi^{(1)} | \mu | \Psi^{(0)} \rangle. \quad (18)$$

Through algebraic manipulation of Equation 18 and Equation 1 and recalling the definition of the ground and first excited states to be $|\Psi^{(0)}\rangle = \exp(-i\omega_g t) |g\rangle$ and $|\Psi^{(1)}\rangle =$

$\sum_m a_m^{(1)}(t) \exp(-i\omega_m t) |m\rangle$ respectively, the linear polarizability is found to be

$$\alpha \equiv \hbar^{-1} \sum_m \frac{\mu_{mg}\mu_{gm}}{\omega_{mg} - \omega_p} + \frac{\mu_{gm}\mu_{mg}}{\omega_{mg}^* + \omega_p}. \quad (19)$$

A damping term must be included in the transition frequency to account for decay within the excited state $|m\rangle$. The damping term [21] is added to the transition frequency such that

$$\omega_{mg}^* = \omega_m - \omega_g - i\Gamma \quad (20)$$

where ω_m , ω_g , and Γ are real and $-i\Gamma$ satisfies the requirement states must decay for $\Gamma > 0$ (i.e. only the ground state is stable). The use of Γ requires the population of excited states remains insignificant in comparison to the ground state. Equation 19 and the following Equation 22 are valid for any field frequencies [21] and the damping term can be ignored except on resonance to avoid divergence.

While the linear polarizability is first order in the applied electric field and second order in the perturbed parameter the second hyperpolarizability is third order in the applied field and fourth order in the perturbed parameter. To solve for the second hyperpolarizability the dipole moment per atom

$$\langle \mu^{(3)} \rangle = \langle \Psi^{(0)} | \mu | \Psi^{(3)} \rangle + \langle \Psi^{(1)} | \mu | \Psi^{(2)} \rangle + \langle \Psi^{(2)} | \mu | \Psi^{(1)} \rangle + \langle \Psi^{(3)} | \mu | \Psi^{(0)} \rangle \quad (21)$$

must be solved once the states $|\Psi^{(2)}\rangle$ and $|\Psi^{(3)}\rangle$ are found using Equation 14.

The second hyperpolarizability for a non-polar molecule (i.e. a molecule with no permanent dipole contribution) can be described by the following off resonance sum-over-states

expression [22]

$$\gamma_{\alpha\beta\gamma\delta}(-\omega_\sigma; \omega_1, \omega_2, \omega_3) = \hbar^{-3} \sum_P \left\{ \sum_{m,n,p} \frac{\langle g|\mu_\alpha|m\rangle \langle m|\mu_\delta|n\rangle \langle n|\mu_\gamma|p\rangle \langle p|\mu_\beta|g\rangle}{(\omega_{mg} - \omega_\sigma)(\omega_{ng} - \omega_1 - \omega_2)(\omega_{pg} - \omega_1)} - \sum_{m,n \neq g} \frac{\langle g|\mu_\alpha|m\rangle \langle m|\mu_\delta|g\rangle \langle g|\mu_\gamma|n\rangle \langle n|\mu_\beta|g\rangle}{(\omega_{mg} - \omega_\sigma)(\omega_{ng} - \omega_1)(\omega_{ng} + \omega_2)} \right\}, \quad (22)$$

where $\omega_\sigma = \omega_1 + \omega_2 + \omega_3$, $|g\rangle$ is the initial ground state of the system, the states $|m\rangle$, $|p\rangle$, $|n\rangle$ are excited electronic or vibrational states, and for H_2 the states $|m\rangle$ and $|p\rangle$ must be electronic excited states to account for wavefunction symmetry. Further, μ_α denotes the α Cartesian component of the electric dipole operator μ , and \sum_P denotes the summation of the 24 terms arising from permuting frequencies with their associated spatial subscripts. For clarity the listed number of terms (pairs) are specific to ESHG and the pairs are $(\mu_\alpha, \omega_{-\sigma})$, $(\mu_\beta, \omega_1), \dots, (\mu_\delta, \omega_3)$. The above expression can be used to isolate the electronic, vibrational, and rotational contributions to γ by means of identifying and grouping the lowest resonance frequency for each term with such resonance being electronic, vibrational, or rotational.

Since the molecule under investigation, H_2 , is a linear homonuclear diatomic molecule, the dipole matrix elements between rovibrational states in the ground electronic state vanish by symmetry as $\langle g|\mu_\alpha|m\rangle \langle m|\mu_\beta|g\rangle = 0$ when $|m\rangle$ is a ground vibrational state. The only terms expressing vibrational contribution are found in the first fraction of Equation 22. This reduction leads to the following vibrational contribution equation

$$\gamma_{\alpha\beta\gamma\delta}^v(-\omega_\sigma; \omega_1, \omega_2, \omega_3) = \hbar^{-3} \sum_P \sum_{n(\neq g)} \frac{1}{(\omega_{ng} - \omega_1 - \omega_2)} \left\{ \sum_{m(\neq g)} \frac{\langle g|\mu_\alpha|m\rangle \langle m|\mu_\delta|n\rangle}{(\omega_{mg} - \omega_\sigma)} \right\} \times \left\{ \sum_{p(\neq g)} \frac{\langle n|\mu_\gamma|p\rangle \langle p|\mu_\beta|g\rangle}{(\omega_{pg} - \omega_1)} \right\}, \quad (23)$$

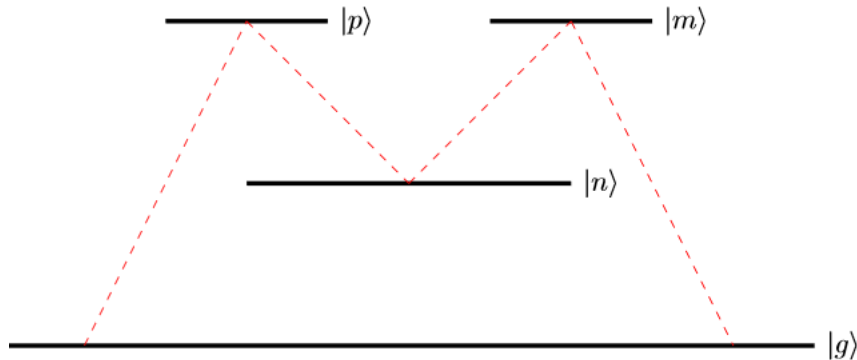


Figure 2: Energy level diagram with states,
 $|g\rangle = |e, v\rangle$
 $|m\rangle, |p\rangle = |e'', v''\rangle$
 $|n\rangle = |e, v'\rangle$
 where $e'' \neq e$
 and $v' \neq v$
 The dashed line follows transitions expressed in Equation 23

where the vibrational transition frequency is ω_{ng} , while the electronic transition frequencies ω_{mg} and ω_{pg} are from the ground electronic manifold. The matrices in the brackets follow the transition dipole moment and can be replaced by Raman transition polarizabilities [22]. As mentioned before, the states $|m\rangle, |n\rangle, |p\rangle$ are excited states while $|g\rangle$ denotes the (initial) ground state (see Figure 2.1).

Since there are many components involved in Equation 23 and not enough ways to evaluate each component, focus was paid to what is experimentally accessible. Two different equations are then derived from the vibrational hyperpolarizability expression using different approximations.

2.2 Approximation, Q-Branch, S-branch, O-branch γ^v

The first approximation begins by treating the optical frequencies $\omega_1, \omega_2, \omega_3$ in Equation 23 as negligible in comparison to the electronic transition frequencies (ω_{mg}). This approximation is justified as electronic transition frequencies ($100,000 \text{ cm}^{-1}$) are well above the measured second overtone ($11,765 \text{ cm}^{-1}$) for H_2 . The next step is to sum over all permuting pairs of dipole moments.

Applying the above method to the vibrational hyperpolarizability expression of Equation 23 leads to the following averaged vibrational hyperpolarizability equation in the lab frame

of reference

$$\begin{aligned}
\langle \gamma^v \rangle_{AB\Gamma\Delta} &= \gamma_{AB\Gamma\Delta}^v(-\omega_\sigma; \omega_1, \omega_2, \omega_3) = \\
& \frac{1}{\hbar} \sum_{v, v' (\neq v)} \sum_J \times \left\{ \frac{1}{30} \left[\frac{(J+1)(J+2)}{(2J+1)(2J+3)} \rho(v, J) \Delta \alpha_{vJ, v'J+2}^2 6\mathbb{D}^2(\omega_{vJ, v'J+2}) \right. \right. \\
& \quad \left. \left. + \frac{(J+1)(J+2)}{(2J+3)(2J+5)} \rho(v, J+2) \Delta \alpha_{vJ+2, v'J}^2 6\mathbb{D}^2(\omega_{vJ+2, v'J}) \right. \right. \\
& \left. \left. + \frac{2}{3} \frac{J(J+1)}{(2J-1)(2J+3)} \rho(v, J) \Delta \alpha_{vJ, v'J}^2 6\mathbb{D}^2(\omega_{vJ, v'J}) \right] \rho(v, J) \alpha_{vJ, v'J}^2 3\mathbb{D}^0(\omega_{vJ, v'J}) \right\}, \quad (24)
\end{aligned}$$

where $\omega_{v,J}$ denotes the transition frequency of states with vibration and rotation quantum numbers v, J and $\rho(v, J)$ are the normalized populations for state $|v, J\rangle$. The factor \mathbb{D} contains all frequency and polarization dependencies of γ^v and whose source and derivation are beyond the scope of this thesis. The derivation can be found in ‘‘Vibrational Contributions to the Hyperpolarizabilities of Homonuclear Diatomic Molecules’’ [22].

Equation 24 is isotropic averaged and so the only independent tensor components are $A, B, \Gamma, \Delta = \text{xxxx}$ and $A, B, \Gamma, \Delta = \text{xyyx}$ for ESHG. The tensor components xxxx and xyyx correspond to the optical and static electric fields polarized parallel and perpendicular to each other respectively. For the one-photon resonance at the $Q(J)$ transitions being investigated, Equation 24 becomes

$$\gamma_{\parallel, Q}^v = \rho(J) \frac{2}{\hbar(\omega_{0J, vJ} - \omega)} \left[\alpha_{0J, vJ}^2 + \frac{4}{45} \frac{J(J+1)}{(2J-1)(2J+3)} \Delta \alpha_{0J, vJ}^2 \right] \quad (25)$$

$$\gamma_{\perp, Q}^v = \rho(J) \frac{2}{\hbar(\omega_{0J, vJ} - \omega)} \left[\frac{1}{15} \frac{J(J+1)}{(2J-1)(2J+3)} \Delta \alpha_{0J, vJ}^2 \right] \quad (26)$$

where in relation to the molecular axis, the anisotropy and isotropy of the polarizabilities are expressed as $\Delta\alpha = (\alpha_{\parallel} - \alpha_{\perp})$ and $\alpha = \frac{(\alpha_{\parallel} + 2\alpha_{\perp})}{3}$, respectively. For pure vibrational transitions $(v, J \rightarrow v', J)$ the values of the transition polarizabilities α_{\parallel} and α_{\perp} for H_2 are found in Hunt

et al.'s “*Ab initio* Calculation of Properties of the Neutral Diatomic Hydrogen Molecules H₂, HD, D₂, HT, DT, and T₂” [23].

The same one-photon equation can be found for the $O(J)$ and $S(J)$ transitions where $v, J \rightarrow v, J \pm 2$ and they are,

$$\gamma_{\parallel,O}^v = \frac{4}{3}\gamma_{\perp,O}^v = \rho(J) \frac{2}{\hbar(\omega_{0J,vJ-2} - \omega)} \left[\frac{2}{15} \frac{J(J-1)}{(2J-1)(2J-3)} \Delta\alpha_{0J,vJ-2}^2 \right] \quad (27)$$

$$\gamma_{\parallel,S}^v = \frac{4}{3}\gamma_{\perp,S}^v = \rho(J) \frac{2}{\hbar(\omega_{0J,vJ+2} - \omega)} \left[\frac{2}{15} \frac{(J+1)(J+2)}{(2J-1)(2J+3)} \Delta\alpha_{0J,vJ+2}^2 \right] \quad (28)$$

The magnitude of response for the vibrational hyperpolarizability for $Q(J)_{\perp}$ is roughly as large as, or larger than, those of the $S(J)$ and $O(J)$ transitions. This is due to there being no isotropic contribution to the hyperpolarizability for these transitions.

2.3 On Resonance: γ_{res}^v

The second hyperpolarizability can be expressed in terms of transition dipole moments where beginning with Equation 23, only consideration of frequencies near the vibrational transition frequency $\omega_{ng} \gg |\omega_{ng} - \omega|$ are made. Focusing on just terms near ω_{ng} and ignoring the spatial indices $\alpha, \beta, \gamma, \delta$, the 24 frequency permutations are then collected. This leads to the following ESHG resonance expression,

$$\gamma_{res}^v(-2\omega; \omega, \omega, 0) = \frac{2}{\hbar(\omega_{ng} - \omega)} \left\{ \sum_{m(\neq g)} \frac{2\mu_{gm}\mu_{mn}}{\hbar(\omega_{mg} + 2\omega)} \right\} \times \left\{ \sum_{p(\neq g)} \frac{2\mu_{gp}\mu_{pn}}{\hbar(\omega_{pg} - \omega)} \right\} \quad (29)$$

Equation 29 is for molecular frame Cartesian components and is exact for the cases of $\alpha, \beta, \gamma, \delta = \text{xxxx}$ and zzzz with z being the molecular axis, since all permutations are the same for these components. The expressions for the remaining independent non-zero molecular components ($\alpha, \beta, \gamma, \delta = \text{zxxz}, \text{xzzx}, \text{zzxx}, \text{xxzz}, \text{xyyx}$) are more complex and

will not be discussed.

2.4 Static and Dynamic Polarizabilities

When a molecule is introduced to an external electric field, the polarization of the molecule can change due to manipulation of the electrons by the applied field (such change is molecule specific [24]), this change is denoted by the effective polarizability α_γ . The effective polarizability for γ_{res}^v can be calculated by

$$\alpha_\gamma = \sqrt{\left\{ \sum_{m(\neq g)} \frac{2\mu_{gm}\mu_{mn}}{\hbar(\omega_{mg} + 2\omega)} \right\} \times \left\{ \sum_{p(\neq g)} \frac{2\mu_{gp}\mu_{pn}}{\hbar(\omega_{pg} - \omega)} \right\}}. \quad (30)$$

Equation 30 is the square root of the product of the two transition polarizabilities of the γ_{res}^v equation. The dispersion for α_γ is the geometric mean of the resonance denominators. Looking at the dispersion of α_γ shows that for frequencies of $\omega_{mg} > 4\omega$, the effective polarizability will decrease as frequency decreases.

The static and dynamic (Raman) polarizability of H_2 can also be related to the γ_{res}^v expression through comparison. Beginning with defining static polarizability using the sum-over-states method [25]

$$\alpha_{\alpha\beta}(0) = 2 \sum_{m(\neq g)} \frac{\mu_{gm}^\alpha \mu_{mn}^\beta}{\hbar\omega_{gn}}. \quad (31)$$

The transition dipole moment is generated from the ground state $|g\rangle$ to the excited state $|n\rangle$. The denominator $\hbar\omega_{gn}$ is the transition energy. Using the same notation, the dynamic polarizability can be expressed as

$$\alpha_{\alpha\beta}(\omega) = \sum_{m(\neq g)} \left\{ \frac{\mu_{gm}^\alpha \mu_{mg}^\beta}{(\hbar\omega_{mg} + \hbar\omega)} + \frac{\mu_{gm}^\alpha \mu_{mg}^\beta}{(\hbar\omega_{mg} - \hbar\omega)} \right\}. \quad (32)$$

Considering tensor orientation requirements discussed above and that for Raman scattering the Stokes frequency is defined as $\omega_S = \omega_P - \omega_{ng}$, with pump frequency ω_P , the static and

dynamic (Raman) polarizabilities can respectively be written as

$$\alpha_0 = \sum_{m(\neq g)} \left\{ \frac{2\mu_{gm}\mu_{mn}}{\hbar\omega_{mg}} \right\} \quad (33)$$

and

$$\alpha_R(-\omega_S; \omega_P) = \sum_{m(\neq g)} \left\{ \frac{\omega_{gm}\omega_{mn}}{\hbar(\omega_{mg} + \omega_S)} + \frac{\omega_{gm}\omega_{mn}}{\hbar(\omega_{mg} - \omega_P)} \right\}. \quad (34)$$

Dispersion of the Raman polarizability is given by the arithmetic mean of the resonance denominators in α_R . This indicates that as the frequency increases, Raman polarizability will increase, since $\omega_S < \omega_P$.

3 Experimental Design

The purpose of this chapter is to explain the experimental set-up, equipment resolution, and how measurements were taken. The chapter begins with an explanation of ring cavity set up as well as the schematic diagram presented in Figure 4. It moves on to explain ways in which noise was reduced since the signal size is exceptionally small (≈ 40 to 300 counts per second) and frequency dependent. To increase signal size, periodic phase matching was employed. Periodic phase matching will be expanded upon along with an explanation of measurement techniques used.

3.1 Design and Set Up

The laser used was a continuous wave Schwartz Electro-Optics Titan CWBB titanium sapphire (CW Ti:S) laser pumped with a Coherent Verdi (532 nm) five watt laser. The Ti:S output beam was, on average, 400 mW for the measured 11600 to 11800 cm^{-1} range. The folded linear resonator is converted to a planar ring by rotating mirrors M3 and M4 (see Figure 3). Then the ring resonator is made into a non-planar ring resonator by raising M3 and the beam path at mirror M3 by 2 cm, and a Faraday rotator is inserted to enforce unidirectional operation. The linear polarization of the resonator mode rotates on each circuit of the non-planar ring and introduces an excess loss at the Brewster angle surfaces of the Ti:S crystal and the birefringent filter. However the introduction of the Faraday rotator (FR) cancels the polarization rotation and excess loss for the beam propagating in one direction (and not the other direction) [26] [27]. The polarization rotation is doubled and excess loss prevents lasing for the mode propagating in the opposite direction.

The longitudinal mode spacing (beat note frequency) is increased from 198 to 240 MHz when the laser was converted from the folded linear to the ring configuration. Single longitudinal mode operation was required to avoid unintended modifications of the ESHG signal [28] [29], and any measurements with the appearance of inter-mode beat notes were rejected.

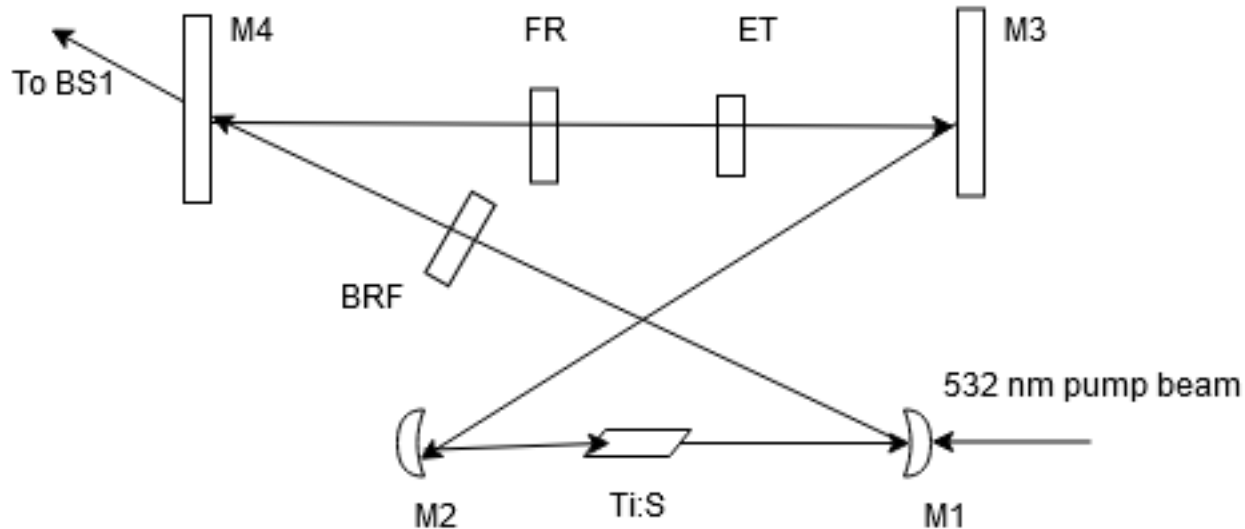


Figure 3: Schematic diagram of the laser cavity described in the text.

The free spectral range of the Ti:S birefringent filter was 150 nm while an additional silica etalon of thickness 1.686 mm and free spectral range of 2 cm^{-1} was used to tune the laser to 0.01 cm^{-1} . Mode monitoring of the laser was achieved using a Fabry-Pérot interferometer and with an RF spectrum analyzer to observe beat notes of the laser output during the entire experiment.

The experimental set-up is illustrated in Figure 4. The beam travels the following path upon exiting the cavity. It is immediately partitioned using beam sampler one (BS1) and then again by beam sampler 4 (BS4), the beam is fiber coupled the beam into a Burleigh WA-20 wavemeter (WM) with a resolution of 0.01 cm^{-1} and is also fiber coupled to a scanning Fabry-Pérot of resolution for mode observation. The wavemeter is a Michelson interferometer under vacuum.

From beam sampler 1 (BS1) the beam is again partitioned by beam sampler 2 (BS2) and immediately focused by Lens 5 (L5) onto a 5GHz InGaAs photodiode (PD) that feeds directly to the RF spectrum analyzer. The beam is then collimated using Lens 1 (L1) and the desired linear polarization is selected using the half-wave plate (HWP) and prism polarizer (POL). Once the desired polarization was prepared, the beam waist was focused to the center

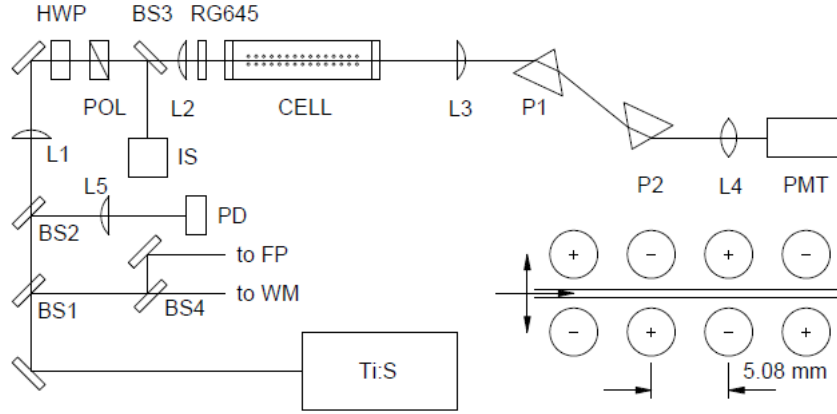


Figure 4: Schematic diagram of the apparatus described in the text. The insert shows the path of the focused linear polarized laser beam between the alternating polarity cylindrical electrodes in the gas cell.

of the cell (CELL) by Lens 2 (L2) with a confocal parameter of 20 cm. Centering the beam waist allows for minimum beam clipping and diffraction by the electrode array. A red glass filter (RG645) was paired with L2 to remove any light at the second harmonic wavelength generated prior to the cell.

The cell is composed of two windows each with a tilt angle of 2 degrees to avoid reflections mixing into the incident beam. The electrode array consists of $N=82$ electrode pairs with a period of 5.08 mm, setting an upper-bound for beam size to avoid clipping anywhere within the cell. The cell was then filled with H_2 gas with a purity of 99.999% achieved through multiple cleaning cycles of the cell. To achieve optimal ESHG signal phase matching was required. The application of a static electric field, ± 6 kV/mm, allows for a larger second harmonic signal; voltage size is restricted to the breakdown voltage of the H_2 gas [30].

Power loss was roughly 1% at each beam sampler. The power was measured after the half-wave plate and polarizer pair to account for higher power loss from the duo. The beam, upon transmitting through the polarizer, was partitioned by beam sampler 3 (BS3) and directed into an integrating sphere (IS) and photodetector. This allows for power measurements to be

taken simultaneously during ESHG signal measurements. The power was measured during ESHG measurements and varied less than 1 mW during the duration of measurements.

The transmitted beam through the cell consists of the fundamental beam and ESHG generated beam which are both collimated by Lens 3 (L3) and then separated by the tandem Brewster prism spectrometer (P1, P2). The ESHG beam is expanded by Lens 4 (L4) before reaching the photocathode of the photomultiplier tube (PMT). The bialkali photocathode used has a quantum efficiency of $\sim 0.001\%$ for the fundamental beam frequency (11765 cm^{-1}) and $\sim 25\%$ for the ESHG frequency (23584 cm^{-1})[31]. Due to the low quantum efficiency of the photocathode for the fundamental beam frequency, no additional filters were necessary for beam separation.

Care was taken to avoid any etalon effects created by optical equipment beyond BS3 by tilting everything save for the electrode array. Tilting avoids any reflected beams overlapping to create etalon fringes. The expansion of the beam with L4 guarantees no etalon effects are generated at the photocathode.

3.2 Signal Collection: Photon Counting Statistics

The technique of photon counting statistics was used for measurements and errors on measurements. For a photon incident upon the photocathode, a photoelectron can be ejected from the photocathode surface, the ejected photoelectron is amplified by secondary emission at the PMT dynodes, and collected by the PMT's anode. Upon collection and output by the anode, the signal is registered by the multi-channel scaler. Ideally each electrical pulse corresponds to a single photoelectron. The arrival of photons is random in time and therefore the number of photon counts in a given interval is not constant. This fluctuation of registered photons is referred to as shot noise and is a fundamental feature of the photoelectric process [32]. In addition to shot noise there is intensity fluctuations of the incident beam and dark counts.

Dark counts are predominantly created by the amplification of thermally released elec-

trons at the photocathode or first dynode and cannot be distinguished from photoelectron pulses. Dark counts exist regardless of incident light and can be reduced with cooling of the PMT. For this experiment background was measured by blocking the fundamental beam and was found to be on average 0.6 counts per second with an uncooled PMT. The measurement of background includes the dark count of the PMT and since background was 0.15% of the signal for $Q_{\parallel}(1)$ no additional steps were taken to reduce dark count.

Errors on the data points were shot noise using the signal to noise ratio,

$$SNR = \frac{N}{\sqrt{N}}. \quad (35)$$

3.3 Measurement Process: Singlets, Triplets, and Power

The term ‘triplet’ refers to the act of measuring the ESHG signal at a reference point, an unspecified point (signal), and the reference point again, all measured in immediate succession (within 2 minutes for changing frequency). The average of the reference points was calculated and used to normalize the signal. For triplets, the ESHG signal and the incident beam power were measured for 100 seconds.

The term ‘singlet’ refers to the act of measuring the ESHG signal at a single unspecified frequency designated as the signal along the resonance curve. Measurement of a reference point in this instance was not done due to the signal size being over ten times smaller than $Q_{\parallel}(1)$ even with a longer measurement duration. For singlet measurements, the ESHG signal and the incident beam power were measured for 300 seconds.

To account for power fluctuations over the measured frequency range, the square power of the incident beam ($P^{(\omega)}$) was divided out of the ESHG signal ($S^{(2\omega)}$). Background was measured (0.6 counts per second on average) and was subtracted from the measured signal. This describes how wide and narrow range frequencies were treated in Figure 5 and Figure 6.

3.4 Coherent Background

Second harmonic generation can occur at the surface of prism 1 which will not be discriminated against by the PMT. To avoid over-counting of second harmonic signals, the coherent background was measured by adjusting the polarity of the gas cell. The total signal measured can be described by the sum of the ESHG generated signal and the coherent background,

$$S_{\pm} \propto (\pm E_s + E_b \cos \phi)^2 \quad (36)$$

where S_{\pm} is the signal generated with positive or negative polarity, E_s is the electric field amplitude of the ESHG signal, and $E_b \cos \phi$ is the electric field amplitude of the coherent background with ϕ phase shift. To measure the coherent background, the ratio of the positive and negative signals is used. Using Equation 36 and some algebraic manipulation leads to the ratio,

$$\frac{S_+}{S_-} = 1 + \frac{4E_s}{E_b \cos \phi} \Leftrightarrow \frac{E_b \cos \phi}{E_s} = \frac{1}{4} \left[\frac{S_+}{S_-} - 1 \right] \quad (37)$$

The measured amplitude of the coherent background of the total signal for Q(1) was found to be $|\frac{E_b \cos \phi}{E_s}| < 0.07\%$. So, of the 300+ counts per second, less than 0.2 counts were coherent background. The coherent background contribution was of the same order for all transitions.

3.5 Electric Field Induced Second Harmonic Generation, Phase-match Peak

Electric field induced second harmonic generation (ESHG) needs to be briefly described in order to understand the influences on the measured signal. Periodic phase matching is a process where an electrode array of N electrodes is used to increase the generated second harmonic signal by a factor of nearly N^2 [33]. Such an increase is made possible by matching the coherence length of the gas sample to the spatial periodicity of the array. This matching

is accomplished by adjusting the density of the gas ρ which is proportional to the wave vector mismatch (Δk) and where,

$$\Delta k = 2k_\omega - k_{2\omega} = \frac{4\pi}{\lambda_\omega}(n_\omega - n_{2\omega}) = -\frac{2\pi}{\lambda_\omega \epsilon_\omega}(\alpha_{2\omega} - \alpha_\omega)\rho + (\dots)\rho^2 \quad (38)$$

The power of the measured second harmonic signal can be expressed as a function of the incident power $P^{(\omega)}$, the applied static electric field $\mathbf{E}_0^{(0)}$, the nonlinear susceptibility of the gas χ_{NL} , the parameters of the electrode array length L , and the confocal parameter $z_0 (= \pi r_0 \frac{n_\omega}{\lambda_0})$ of the beam. The ESHG power is then,

$$P_{opt}^{(2\omega)} = \frac{\omega^3}{\pi c n_{2\omega}^2} \left[\frac{\mu_0}{\epsilon_0} \right]^{3/2} \chi_{NL}^2 \left(P^{(\omega)} \mathbf{E}_0^{(0)} \right)^2 L \left[\frac{z_0}{L} \arctan^2 \left(\frac{L}{z_0} \right) C \left(\frac{L}{z_0} \right) \right] \quad (39)$$

For this experiment's range of measured frequencies, the static electric field remains constant, the confocal parameter change is negligible, and the length of the array remains constant. The size of χ_{NL} will vary proportionally to density and for H_2 the relationship between the microscopic second hyperpolarizability and the macroscopic susceptibility was shown in Equation 2. This relationship establishes the importance of density for the macroscopic susceptibility and the ESHG signal. While it would be beneficial to have a high density, there is an upper-bound set by the phase match requirement. As phase match is frequency and density dependent, the density was matched for a frequency less than roughly 1 cm^{-1} away from the expected resonance frequency using,

$$\frac{p_1}{p_2} \propto \left(\frac{\nu_2}{\nu_1} \right)^3. \quad (40)$$

Since the temperature of the room and the temperature of the cell fluctuate, the pressure of the gas was measured before closing off the cell. With the density held constant, the signal was taken over a broad range ($50 - 100 \text{ cm}^{-1}$) to map the phase match peak. Multiple measurements were also taken near the desired resonance ($\geq 2 \text{ cm}^{-1}$ away) to map the phase match peak slope. This was done each time a Q(J) measurement was taken to account for the

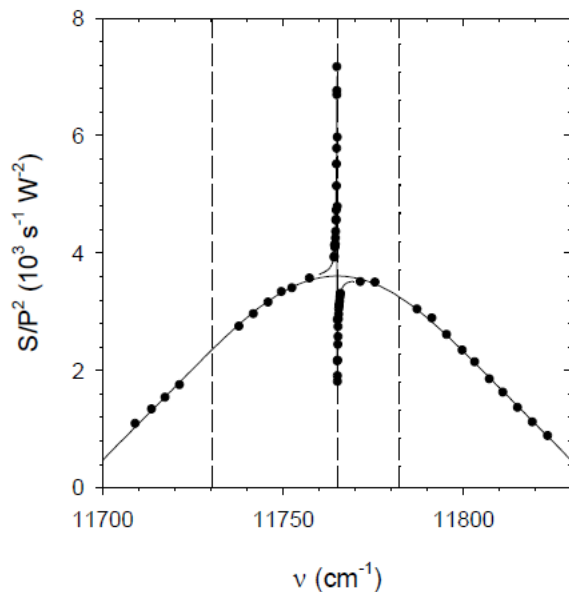


Figure 5: ESHG signal vs frequency measured for the H_2 3-0 Q(1) transition. The solid lines are fits of Equation 42 to the data points. Dashed lines are where Q(2),Q(1),Q(0) fall respectively.

difference between Q(J) transition frequencies and for daily cell leaking. Figure 5 shows the phase match peak for Q(1) over a broad frequency range. The dashed lines, from left to right, represent the Q(2), Q(1), Q(0) resonant frequencies respectively. Although the phase match is set for a particular transition, other transitions will influence the peak shape. To avoid peak shape manipulation by other resonances care was taken to avoid all other resonance frequencies by 5-10 cm^{-1} .

The wide range points were fit to the normalized phase match peak function,

$$g(\nu) = 1 - x^2 + 0.42x^4 - 0.10x^6 \quad (41)$$

where $x = (\nu - \nu_m)/w$ and $w \approx 54 \text{ cm}^{-1}$. The variables ν_m , w , and S_m are parameters (peak

position, width, height) found by fitting the wide scan data points to Equation 41. The solid line in Figure 5 is the function $S_m g(\nu)$ fit to the wide scan data points. The observed second harmonic signal is,

$$\frac{S^{(2\nu)}}{P^2} = Af(\nu)g(\nu) \quad (42)$$

where the function $f(\nu)$ is described in the next section.

3.6 Resonant Fit Function

The second hyperpolarizability is proportional to the generated ESHG signal and can be separated into its resonance and non-resonance parts such that

$$S^{(2\omega)} \propto |\gamma_{nr} + \gamma_{res}^v|^2 = (\gamma_{nr} + \gamma_{res,R}^v)^2 + (\gamma_{res,I}^v)^2. \quad (43)$$

By representing the (vibrational) hyperpolarizability as a combination of its real and imaginary resonant parts and its non-resonant parts, calibration of γ_{res}^v can be done using the well studied γ_{nr} [34]. Beginning with the anti-Stokes spectrum [35], and through some algebraic manipulation, the experimental resonant fit function is

$$f(\nu) = \left(1 + \frac{a(b - \nu)}{(b - \nu)^2 + c^2}\right)^2 + \left(\frac{ac}{(b - \nu)^2 + c^2}\right)^2, \quad (44)$$

with the experimentally determined parameters being defined as the following: a is the relative amplitude of γ_{res}/γ_{nr} , b is the resonance frequency, and c is the resonance width. Experimentally a , b , c , and ν have units of cm^{-1} . The narrow range resonance in Figure 6 is fit to Equation 44.

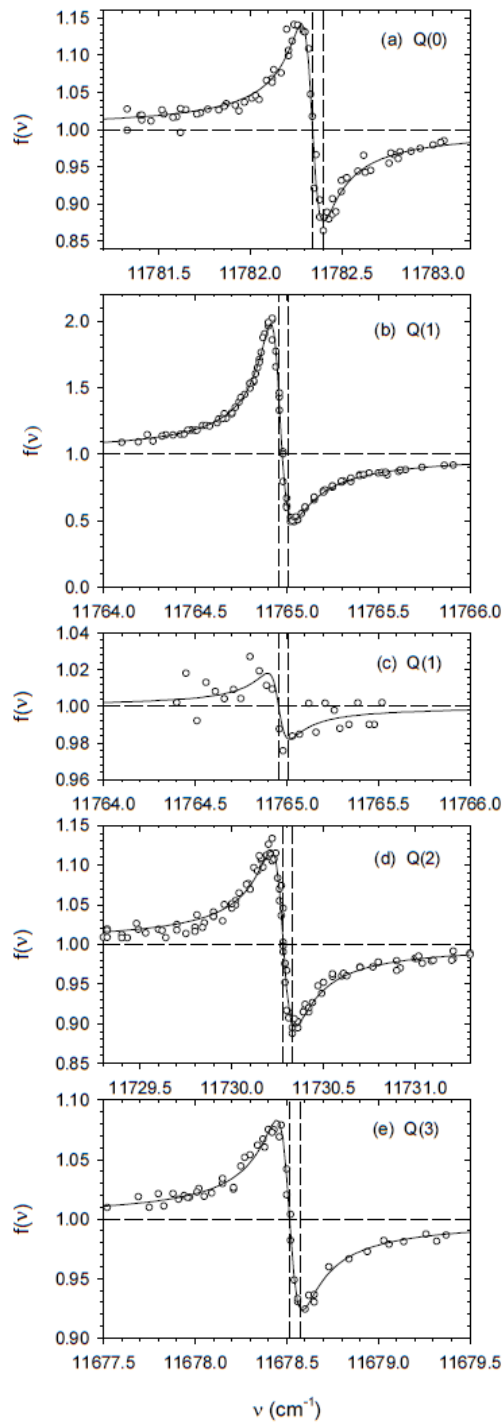


Figure 6: Overtone resonance spectra over 2 cm^{-1} for H_2 transitions (a) $\text{Q}(0)_{\parallel}$, (b) $\text{Q}(1)_{\parallel}$, (c) $\text{Q}(1)_{\perp}$, (d) $\text{Q}(2)_{\parallel}$, and (e) $\text{Q}(3)_{\parallel}$. \parallel and \perp denote parallel and perpendicular polarization respectively. The solid curves are fits of Equation 44 to the data points. The vertical dashed lines are measured and *ab initio* resonance frequencies. The horizontal dashed lines mark the non-resonant background contribution.

Table 3: Experimental results of the fit function Equation 44

Transition	a (10^{-3}cm^{-1})	b (cm^{-1})	c (10^{-3}cm^{-1})
3-0 Q(0)	7.85 ± 0.27	11782.338 ± 0.001	58.9 ± 2.5
3-0 Q(1)	40.87 ± 0.65	11764.956 ± 0.001	59.1 ± 1.0
3-0 Q $_{\perp}^a$ (1)	1.06 ± 0.17		
3-0 Q(2)	7.20 ± 0.26	11730.278 ± 0.001	64.9 ± 2.5
3-0 Q(3)	5.49 ± 0.23	11678.513 ± 0.002	68.5 ± 2.9

a: the value of a for 3-0 Q(1) $_{\perp}$ was found by setting the values for b and c to those of 3-0 Q(1) $_{\parallel}$.

4 Analysis and Results

The analysis and results section is set up as follows: an introduction to collision broadening and how it has been measured and calculated, phase match densities and how they are measured and calculated, the non-resonant contribution to γ and how to calculate it, and finally the measured value of the hyperpolarizability and a subsequent theoretical comparison.

4.1 Collisional Broadening

The environment necessary for ESHG generation for a light gas such as hydrogen requires pressure densities of $\rho = 406 \text{ mol m}^{-3}$ (9.11 amagat). With such a high density, the perturbation of the molecules will influence the line-shape of their neighbors. The resonance frequency widths are proportional to the density of the gas as expressed by the fitted function in Owyong’s “High-Resolution CW Stimulated Raman Spectroscopy in Molecular Hydrogen” [36].

There has been extensive research on collisional broadening due to its effects on spectroscopic resolution [37] [38]. This thesis benefits from previous H_2 self-broadening measurements for the Q(0-5) transitions by Rahn, Farrow, and Rosasco and the work of Bragg, Brault, and Smith which are summarized in Table 4. The *ab initio* zero pressure broadening obtained from Brault et al. was used to calculate frequency shifting for the Q(J) transitions measured in this work. Table 4 gives a list of values from Rahn et al, Brault et al, and this experiment and should be consulted when analysing the legitimacy of the resonant fit function. Figure 7 shows the pressure shift and broadening coefficients plotted for different Q-branch frequencies.

4.2 Effective Polarizability and Non-Resonance Response

The relative amplitude, a , can be calculated using the effective polarizability, the non-resonant hyperpolarizability γ_{nr} at that particular transition frequency, and the population

Table 4: Pressure shift and broadening coefficients measured for H₂ vibration transitions.

Transition	ν_0^a (cm ⁻¹)	ρ^b (amagat)	$\frac{(\nu_0-b)}{\rho^c}$ (10 ³ cm ⁻¹ amagat ⁻¹)	$\frac{c}{\rho^d}$ (10 ⁻³ cm ⁻¹ amagat ⁻¹)
1-0 Q(0)	4161.168 4			1.33 ± 0.01
1-0 Q(1)	4155.254 7		2.13 ± 0.04	0.87 ± 0.04
1-0 Q(2)	4143.466 0		2.0 ± 0.1	1.48 ± 0.01
1-0 Q(3)	4125.873 9		2.2 ± 0.2	1.21 ± 0.01
1-0 Q(4)	4102.582 0		1.7 ± 1.9	1.71 ± 0.03
1-0 Q(5)	4073.732 7			1.17 ± 0.03
2-0 Q(1)	8075.311 4		4.8 ± 0.2	
2-0 Q(2)	8051.991 0		4 ± 3	
2-0 Q(3)	8017.190 0		4 ± 4	
3-0 Q(0)	11782.397 1	9.059	6.6 ± 1.1	6.5 ± 0.3
3-0 Q(1)	11765.007 8	9.108	5.7 ± 1.1	6.5 ± 0.1
3-0 Q(2)	11730.331 8	9.192	5.9 ± 1.1	7.1 ± 0.3
3-0 Q(3)	11678.572 1	9.328	6.3 ± 1.1	7.3 ± 0.3

a: ν_0 from Ref. [39]

b: 1 amagat = $\rho_{STP} = 44.588$ mol/m³ for H₂ gas.

c: Shift for 1–0 and 2–0 from Ref. [37]

d: Broadening for 1–0 from Ref. [38].

density $\rho(J)$ of rotational state J , where $\rho(J) \propto (2J + 1)g_{ns}(J)\exp(\frac{E_{0J}}{k_B T})$. The calculated strength of the relative amplitude is then,

$$a_{calc} = \frac{\rho(J)\alpha_{eff}^2 e_H}{\gamma_{nr}}. \quad (45)$$

Each transition's calculated amplitude is in Table 6. To account for detuning of the molecular system, the equations for one-photon Q-branch transitions being investigated have the damping term, $i\Gamma$, added to the denominators to produce complex hyperpolarizabilities expressed

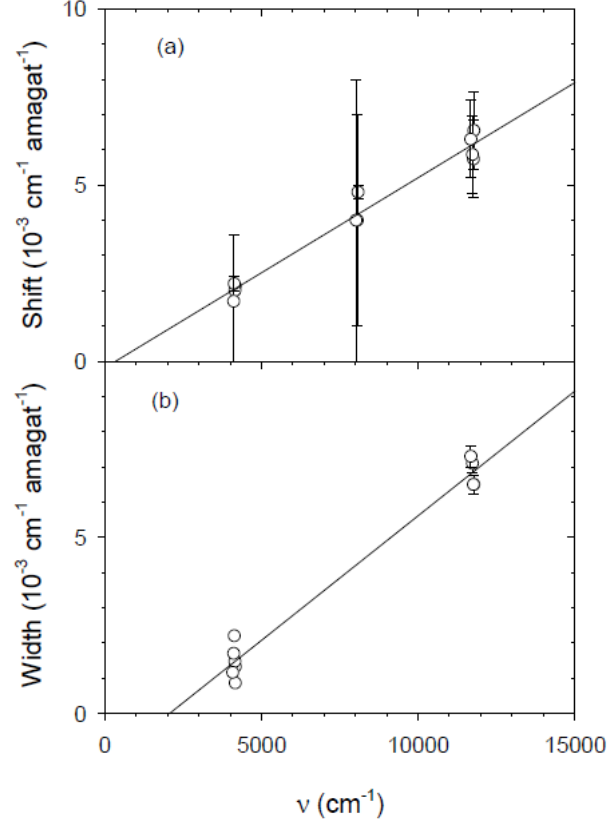


Figure 7: Pressure shift (a) and broadening (b) coefficients plotted vs Q-branch transition frequencies. Lines fit to the data are guides to the eye.

as

$$\gamma_{\parallel,Q}^v = \rho(J) \frac{2}{\hbar} \left[\alpha_{0J,vJ}^2 + \frac{4}{45} \frac{J(J+1)}{(2J-1)(2J+3)} \Delta \alpha_{0J,vJ}^2 \right] \times \left[\frac{(\omega_{0J,vJ} - \omega) - i\Gamma}{(\omega_{0J,vJ} - \omega)^2 + \Gamma^2} \right] \quad (46)$$

$$\gamma_{\perp,Q}^v = \rho(J) \frac{2}{\hbar} \left[\frac{1}{15} \frac{J(J+1)}{(2J-1)(2J+3)} \Delta \alpha_{0J,vJ}^2 \right] \times \left[\frac{(\omega_{0J,vJ} - \omega) - i\Gamma}{(\omega_{0J,vJ} - \omega)^2 + \Gamma^2} \right]. \quad (47)$$

These equations, defined in Section 2.2, are related to the effective polarizability in the

following ways

$$\alpha_{eff,\parallel}^2 = \left[\alpha_{0J,vJ}^2 + \frac{4}{45} \frac{J(J+1)}{(2J-1)(2J+3)} \Delta \alpha_{0J,vJ}^2 \right] \quad (48)$$

$$\alpha_{eff,\perp}^2 = \left[\frac{1}{15} \frac{J(J+1)}{(2J-1)(2J+3)} \Delta \alpha_{0J,vJ}^2 \right]. \quad (49)$$

Another value needed for a_{calc} is the non-resonant hyperpolarizability at each transition. The non-resonant hyperpolarizability response for each transition is calculated using the function

$$\gamma_{nr} = \gamma_0(1 + B\nu_L^2 + C\nu_L^4) + G\nu^{-2} + H\nu^{-4}. \quad (50)$$

The non-resonant hyperpolarizability is found by fitting Equation 50 to previous ESHG measurements, with 0.5% accuracy, made for H₂ over a wide frequency range with parallel polarization [34]. The parameter values for Equation 50 are found in Table 5.

Table 5: Parameters for Equation 50

γ_0 (a.u.)	B (cm ²)	C (cm ⁴)	G ^a (a.u. cm ⁻²)	H ^A (a.u. cm ⁻⁴)
686.41	1.200×10^{10}	2.254×10^{20}	2.55210^9	3.997×10^{16}

a: approximation to the rovibrational contribution off-resonance

4.3 Comparing Relative Strength of Resonance

For appropriate comparison, Table 6 lists the transition and its associated fractional population, isotropic polarization, anisotropic polarization, non-resonant response, calculated vibrational response, and the experimental to calculation fractional deviation. The discrepancies between the calculated and experimental resonance strength follow a trend of being larger than *ab initio* values; the static nature of α_{eff} and Morse potential are investigated in the next two sections.

Table 6: Comparison for experimental and calculated resonance at T=295 K

Transition	J	$\rho(J)$	α (10^{-2} a.u.)	$\Delta\alpha$ (10^{-2} a.u.)	γ_{nr} (a.u.)	a_{calc} (10^{-3}cm^{-1})	a_{exp}/a_{calc}
3-0 Q(0)	0	0.1304	0.993	0.567	745.3	7.57	1.037 ± 0.034
3-0 Q(1)	1	0.6596	0.997	-0.568	745.0	39.08	1.046 ± 0.016
3-0 Q $_{\perp}$ (1)	1	0.6596	0.997	-0.568	256.1	0.97	1.11 ± 0.16
3-0 Q(2)	2	0.1164	1.004	-0.568	744.3	6.98	1.032 ± 0.036
3-0 Q(3)	3	0.0887	1.014	-0.567	743.3	5.43	1.011 ± 0.042

4.4 Data Analysis: Effective Polarizability

The effective polarizability, defined in Equation 30, is static. As the experimental results are dynamic it is beneficial to consider the dispersion of α_{eff} . To estimate the frequency dispersion for γ_{res}^v , α_R , and α_0 , an effective electronic excitation energy is incorporated into their sum over excited electronic states.

The effective excitation energy can be calculated by fitting α_R to the polarizability dispersion of 1-0 Q(1) in Bishop and Pipin [40]. For vertically polarized light, with a frequency of $\hbar\omega = 0.10$ a.u., the Raman polarizability is $\alpha_R = 0.819488$ a.u. and an accompanying static polarizability of $\alpha_0 = 0.749336$ a.u. The ratio, $\frac{\alpha_R}{\alpha_0} = 1.0936$ means that for the 1-0

Q(1) transition the Raman polarizability is 1.094 times larger than the static polarizability. Summing the static polarizability (Eq. 33) and Raman polarizability (Eq. 34) to a single state (ω_{eg}) and taking the ratio leads to,

$$\frac{\alpha_R}{\alpha_0} = \frac{\omega_{eg}}{2} \frac{(2\omega_{eg} - \Delta\omega)}{(\omega_{eg} + \omega_S)(\omega_{eg} - \omega_p)}. \quad (51)$$

By solving for ω_{eg} with a ratio value of 1.0936 an effective electronic transition frequency of $\omega_{eg} = 82000 \text{ cm}^{-1}$ (0.3736 au) is found [41]. To estimate the dispersion for the 3-0 Q(1) transition, $\omega_{eg} = 0.3736 \text{ a.u.}$, $\omega_p = 0.10 \text{ a.u.}$, and the value $\Delta\omega = 11765 \text{ cm}^{-1}$ (0.0536 au) are substituted into Equation 51. The dispersion size found is 0.9525 meaning α_γ is 0.95 times the estimated static value from Equation 30. The a_{calc} values are then over estimated by 10% and the discrepancies between theory and experiment are 14% instead of 4%.

Measurements for 3-0 Q(1) were previously taken and found to be $\frac{\alpha_{0,1;3,1}}{\alpha_{0,1;1,1}} = 1.14 \times 10^{-2}$ [42]. Fitting this collected data to Bishop and Pipin’s [40] *ab initio* values shows a 5% difference between theory and experiment. Further support for 1-0 Q(1) *ab initio* values being underestimated is found in “Raman Chirped Adiabatic Passage: A New Method for Selective Excitation of High Vibrational States” where the effective Raman transition moment was found to be nearly 0.8 a.u. [43] which is orders of magnitude off from *ab initio* calculations.

4.5 Data Analysis: Non-resonant Contributions

As the measured hyperpolarizabilities include the non-resonant hyperpolarizability γ_{nr} contributions, these values must also be investigated. Fitting Equation 50 gives the calculated non-resonant hyperpolarizability contribution for resonant frequency for the parallel components. To find the perpendicular components for 3-0 Q(1), previously measured H₂ data is consulted. Referring to Figure 1 in Shelton and Lu’s “Kleinman Symmetry Deviations for Hydrogen” [44], plotting the the ratio $\frac{\gamma_{||}}{\gamma_{\perp}}$ for 1-0 Q(1) with a frequency value of $\nu_L^2 = 1.04 \times 10^8 \text{ cm}^{-2}$ leads to the ratio $\frac{\gamma_{||}}{\gamma_{\perp}} = 2.909$, meaning the perpendicular measurements are 2.909

times smaller than their parallel counterparts.

Looking at the non-resonant contributions to 3-0 Q(1), the maximum vibrational hyperpolarizability was found to be $|\gamma^v| = 515$ a.u. on resonance and 100 cm^{-1} off resonance $|\gamma^v| = \pm 0.26$ a.u. Comparatively the rovibrational contribution to the non-resonant hyperpolarizability for the 3-0 Q(1) transition was found to be $\gamma_{nr}^{vr} = -20.5$ a.u. and is dominated by the contribution of the far off resonance fundamental vibration transition.

The expression for γ_{nr}^{vr} is derived from Equation 50 and found by neglecting the polarizability factors in Equation 23. While the frequency dependence of γ_{nr}^{vr} is uncertain, there is good agreement between calculations for the fundamental transition polarizabilities [45]. The dispersion for γ_{nr}^{vr} is suggested to be important by the discrepancy between the 1-0 Q(1) Raman polarizability $\nu_p = 11765 \text{ cm}^{-1}$ and the static value with a ratio of 1.044 and would produce a 10% increase of the calculated γ_{nr}^{vr} value for $\nu = 11765 \text{ cm}^{-1}$.

Due to multiple contributions of overtone resonances a simple equation like Equation 50 is not possible for γ^v far off resonance. Support for dispersion of α_{eff} being less than α_R is found in [46], offering accurate experimental results using ESHG and a comparison of *ab initio* results for γ at $\nu = 19430 \text{ cm}^{-1}$ for H_2 . Theory and experiment agree with $\pm 0.1\%$ uncertainty meaning such an agreement 1) indicates the increase of γ_{nr}^{vr} from the dispersion of the effective polarizability is less than 14% and 2) sets an upper-bound on the error for calculated values of γ_{nr}^{vr} .

At $\nu = 19430 \text{ cm}^{-1}$ the hyperpolarizability γ_{nr}^{vr} contributes 0.74% of the total γ value. The uncertainty of γ_{nr}^{vr} does not impact the calculations of γ_{nr} or the accuracy of γ^v for the measured second overtone Q(J) transitions in this experiment since Equation 43 is fit to experimental data. The uncertainty does however impact the separation of the non-resonant hyperpolarizabilities into electronic and rovibrational parts and should be considered for future works.

5 Conclusion

The second overtone vibrational contribution to the second hyperpolarizability of H₂ was measured. Measurements were compared to high level *ab initio* transition polarizabilities in Section 4.4 and found to be 4-14% larger than predicted and indicate that *ab initio* polarizability calculations for $\Delta v=3$ transitions are 2-7% too small. Care was taken to remove systematic errors as outlined in Section 3 and the use of previously measured non-resonant hyperpolarizabilities for H₂ as calibration for the experiment does not discount the large discrepancies as discussed in Section 4.5. The method used in this experiment can be applied to overtone measurements for other small molecules.

References

- [1] K. Iizuka, “History of optics”, in *Engineering Optics* (Springer, New York, NY, 2008), pages 1–24.
- [2] Epicurus and D. Laertius, “Letter to Herodotus”, in *Lives of Eminent Philosophers*, Vol. 2, translated by R. D. Hicks (William Heinemann, London, 1925), pages 565–613.
- [3] F. Ferlin, “New insights into major theoretical research in optics in the age of enlightenment”, *Centaurus* **59**, 308–319 (2017).
- [4] N. Bloembergen, “Nonlinear optics: past, present, and future”, *IEEE Journal of Selected Topics in Quantum Electronics* **6**, 876–880 (2000).
- [5] O. Darrigol, *A history of optics from greek antiquity to the nineteenth century* (Oxford University Press, Oxford, 2012).
- [6] T. Maiman, “Stimulated optical radiation in ruby”, *Nature* **187**, 493–494 (1960).
- [7] M. Göppert-Mayer, “Über elementarakte mit zwei quantensprüngen”, *Annalen der Physik* **401** (1931).
- [8] P. A. Franken, A. E. Hill, C. W. Peters, and G. Weinreich, “Generation of optical harmonics”, *Phys. Rev. Lett.* **7**, 118–119 (1961).
- [9] N. H. Green, R. M. Delaine-Smith, H. J. Askew, R. Byers, G. C. Reilly, and S. J. Matcher, “A new mode of contrast in biological second harmonic generation microscopy”, *Scientific Reports* **7** (2017).
- [10] D. E. Chang, V. Vuletić, and M. D. Lukin, “Quantum nonlinear optics—photon by photon”, *Nature Photonics* **8**, 685–694 (2014).
- [11] E. Garmire, “Nonlinear optics in daily life”, *Optics Express* **21**, 30532–30544 (2013).
- [12] D. C. Hannah, M. A. Yaratic, and D. Cotter, *Nonlinear optics of free atoms and molecules*, Vol. 17, Springer Series in Optical Sciences (Springer, New York, NY, 1979).

- [13] R. W. Boyd, *Nonlinear optics*, Third (Academic Press, Burlington, MA, 2008).
- [14] D. P. Shelton and V. Mizrahi, “Frequency dependence of the hyperpolarizability measured for SF₆”, *Chem. Phys. Lett.* **120**, 318–320 (1985).
- [15] D. P. Shelton and J. E. Rice, “Measurements and calculations of the hyperpolarizabilities of atoms and small molecules in the gas phase”, *Chem. Rev.* **94**, 3–29 (1994).
- [16] M. Born and R. Oppenheimer, “Zur quantentheorie der molekeln”, *Annalen der Physik* **389** (1927).
- [17] R. S. Finn and J. F. Ward, “Dc-induced optical second-harmonic generation in the inert gases”, *Phys. Rev. Lett.* **26**, 285–289 (1971), <https://link.aps.org/doi/10.1103/PhysRevLett.26.285>.
- [18] J. F. Ward and G. H. C. New, “Optical third harmonic generation in gases by a focused laser beam”, *Phys. Rev.* **185**, 57–72 (1969), <https://link.aps.org/doi/10.1103/PhysRev.185.57>.
- [19] P. P. Ho and R. R. Alfano, “Optical kerr effect in liquids”, *Phys. Rev. A* **20**, 2170–2187 (1979), <https://link.aps.org/doi/10.1103/PhysRevA.20.2170>.
- [20] D. M. Bishop, “Molecular vibration and nonlinear optics”, in *Advances in Chemical Physics*, Vol. 104, edited by I. Prigogine and S. A. Rice (Wiley, New York, NY, 1998).
- [21] B. J. Orr and J. F. Ward, “Perturbation theory of the non-linear optical polarization of an isolated system”, *Mol. Phys.* **20**, 513–526 (1971).
- [22] D. P. Shelton, “Vibrational contributions to the hyperpolarizabilities of homonuclear diatomic molecules”, *Mol. Phys.* **60**, 65–76 (1987).
- [23] J. L. Hunt, J. D. Poll, and L. Wolniewicz, “*Ab initio* calculation of properties of the neutral diatomic hydrogen molecules H₂, HD, D₂, HT, DT, and T₂”, *Can. J. Phys.* **62**, 1719–1723 (1984).

- [24] R. Chang, *Physical chemistry for the biosciences* (University Science Books, Sausalito, CA, 2005).
- [25] S. M. Smith, A. N. Markevitch, D. A. Romanov, X. Li, R. J. Levis, and H. B. Schlegel, “Static and dynamic polarizabilities of conjugated molecules and their cations”, *J. Phys. Chem.* **108**, 11063–11072 (2004).
- [26] T. Johnston and W. Proffitt, “Design and performance of a broad-band optical diode to enforce one-direction traveling-wave operation of a ring laser”, *IEEE Journal of Quantum Electronics* **16**, 483–488 (1980).
- [27] D. Welford and M. A. Jaspan, “Single-frequency operation of a cr:ytg laser from 1332 to 1554 nm”, *J. Opt. Soc. Am. B* **21**, 2137–2141 (2004), <http://josab.osa.org/abstract.cfm?URI=josab-21-12-2137>.
- [28] S. Helmfrid and G. Arvidsson, “Second-harmonic generation in quasi-phase-matching waveguides with a multimode pump”, *J. Opt. Soc. Am. B* **8**, 2326–2330 (1991).
- [29] W.-L. Zhou, Y. Mori, T. Sasaki, and S. Nakai, “Theoretical analysis of multimode pumped second-harmonic generation”, *Japanese Journal of Applied Physics* **34**, 5606–5609 (1995).
- [30] Y. Chen, “Electrical breakdown of gases in subatomic pressure”, Master’s thesis (Auburn University, Auburn, AL, Aug. 2016).
- [31] Hamamatsu, *Photomultiplier tubes: Photomultiplier tubes and related products* (Hamamatsu Photonics K.K., Hamamatsu City, Japan, Feb. 2016), https://www.hamamatsu.com/resources/pdf/etd/PMT_TPMZ0002E.pdf.
- [32] P. Koczyk, P. Wiewiór, and C. Radzewicz, “Photon counting statistics—undergraduate experiment”, *American Journal of Physics* **64**, 240–245 (1996), <https://doi.org/10.1119/1.18211>.
- [33] D. P. Shelton, “Construction of a periodic electrode array”, *Rev. Sci. Instrum.* **56**, 1474–1475 (1985).

- [34] D. P. Shelton, “Nonlinear-optical susceptibilities of gases measured at 1064 and 1319 nm”, *Phys. Rev. A* **42**, 2578–2592 (1990).
- [35] Y.-R. Shen, *The principles of nonlinear optics* (Wiley-Interscience, New York, NY, 2002).
- [36] A. Owyong, “High-resolution CW stimulated Raman spectroscopy in molecular hydrogen”, *Opt. Lett.* **2**, 91–93 (1978).
- [37] S. L. Bragg, J. W. Brault, and W. H. Smith, “Line positions and strengths in the H₂ quadrupole spectrum”, *The Astrophysical Journal* **263**, 999–1004 (1982).
- [38] L. A. Rahn, R. L. Farrow, and G. J. Rosasco, “Measurement of the self-broadening of the H₂ Q(0–5) Raman transitions from 295 to 1000 K”, *Phys. Rev. A* **43**, 6075–6088 (1991).
- [39] K. Pachucki and J. Komasa, “Nonadiabatic corrections to rovibrational levels of h₂”, *The Journal of Chemical Physics* **130**, 164113 (2009), <https://doi.org/10.1063/1.3114680>.
- [40] D. M. Bishop and J. Pipin, “Calculated Raman overtone intensities for H₂ and D₂”, *J. Chem. Phys.* **94**, 6073–6080 (1991).
- [41] R. M. Ellis and D. P. Shelton, “Vibration overtone hyperpolarizability measured for H₂”, *J. Chem. Phys.* **152**, 154301.
- [42] D. P. Shelton, “Raman overtone intensities measured for H₂”, *J. Chem. Phys.* **93**, 1491–1495 (1990).
- [43] S. Chelkowski and A. D. Bandrauk, “Raman chirped adiabatic passage: A new method for selective excitation of high vibrational states”, *J. Raman Spectrosc.* **28**, 459–466 (1997).
- [44] D. P. Shelton and Z. Lu, “Kleinman symmetry deviations for hydrogen”, *Phys. Rev. A* **37**, 2231–2233 (1988).

- [45] A. Raj, H.-o. Hamaguchi, and H. A. Witek, “Polarizability tensor invariants of H₂, HD, and D₂”, *J. Chem. Phys.* **148**, 104308 (2018).
- [46] E. A. Donley and D. P. Shelton, “Hyperpolarizabilities measured for interacting molecular pairs”, *Chem. Phys. Lett.* **215**, 156–162 (1993), Erratum-ibid. Donley and Shelton [47].
- [47] E. A. Donley and D. P. Shelton, “Erratum: Hyperpolarizabilities measured for interacting molecular pairs”, *Chem. Phys. Lett.* **228**, 701 (1994).

Curriculum Vitae

Rachel Ellis

4505 S Maryland Pkwy, Las Vegas, NV 89154

emailing.with.rachel@gmail.com

EDUCATION

University of Nevada - Las Vegas

August 2017 - Present

Master in Physics

Department of Physics and Astronomy

University of Nevada - Las Vegas

August 2013 - May 2017

Bachelor in Physics

Department of Physics and Astronomy

PROJECTS

Vibrational Contribution to Hyperpolarizability of H₂

Project aims at measuring the vibrational contributions to the hyperpolarizability of the hydrogen molecule. Focus is paid specifically to the second overtones.

PUBLICATIONS

Ellis R. , Shelton D.P. , J. Chem. Phys. 152, 154301 (2020); <https://doi.org/10.1063/5.0005233>

TECHNICAL STRENGTHS

Modeling and Analysis	SigmaPlot, Mathematica
Software & Tools	MS Office, Latex
Laser Alignment	CW Ti:S system
Financial Literacy	Grant opportunities

WORK EXPERIENCE

Teaching Assistant

August 2017 - Present

One-on-one and group distance learning

PhET simulations (Physics)

EXTRA-CURRICULAR

UNLV Science Fair Judge 2019